sustainability

MDPI

Article

Experimental Study on the Enhancement of Waterproof Performance of Shield Tunnel Joints Using Diatomite–MICP Combined Reinforcement Technology

Yu Liang [1,2,*], Changyu Long [1], Xingzhong Nong [3] and Quan Yuan [3]

[1] School of Civil Engineering, Sun Yat-sen University, Guangzhou 510220, China
[2] State Key Laboratory of Tunnel Engineering, Guangzhou 510220, China
[3] Guangzhou Metro Design & Research Institute Co., Ltd., Guangzhou 510080, China
* Correspondence: liangyu25@mail.sysu.edu.cn

Abstract

With the continuous development of China's economy and technology, the number of urban transportation shield tunnels has been increasing. As tunnel depth and diameter grow, the geological conditions become increasingly complex, making leakage at segment joints of shield tunnels a more prominent issue, significantly affecting the sustainable development of urban transportation. To address the issue of water leakage, microbially induced calcium carbonate precipitation (MICP) technology offers a green and environmentally friendly solution. However, relying solely on MICP technology is insufficient to enhance the waterproofing performance of large segment joints of shield tunnel. To address this, this study proposes combining diatomite as both a carrier and filler material with MICP technology, using a diatomite–MICP composite grout to improve the waterproofing performance of tunnel segment joints. First, through laboratory macro-scale tests and micro-morphology analysis, the influence of diatomite dosage on the sealing performance of diatomite–MICP composite grout was systematically studied, and the optimal diatomite dosage was determined. Based on this, a self-developed segment joint waterproofing testing platform was adopted to conduct hydraulic tests on double-seal gasket joints, evaluating the enhancement effect of the composite grout on the overall waterproofing performance of tunnel segment joints. The results indicated that the dosage of diatomite significantly affects the sealing performance of the composite grout, with an optimal dosage of 20% by weight of the bacterial solution. At this dosage, the composite grout achieved the highest density, resulting in maximum unconfined compressive strength and shear strength, as well as the lowest permeability coefficient. The joint water pressure test confirmed that after grouting with a diatomite–MICP composite grout at the optimal dosage of 20%, the breakdown water pressures of the inner and outer seal gaskets at the segment joints reached 2011 kPa and 2019 kPa, representing increases of 15.91% and 16.64% compared to the control group without grouting. This study demonstrates the effectiveness and application potential of the green biomineralization technologies in waterproofing of shield tunnel joints.

Keywords: MICP; *Bacillus pasteurii*; diatomite; tunnel joints; grouting waterproofing

Check for updates

Academic Editor: Antonio Caggiano

Received: 27 May 2026
Revised: 30 June 2026
Accepted: 1 July 2026
Published: 4 July 2026

Copyright: © 2026 by the authors. Licensee MDPI, Basel, Switzerland. This article is an open access article distributed under the terms and conditions of the Creative Commons Attribution (CC BY) license.

1. Introduction

With economic development, the construction of shield tunnels in urban areas has advanced rapidly. However, water leakage at segment joints has become increasingly prominent during long-term operation, not only weakening structural durability but also

adversely affecting mechanical and electrical equipment within the tunnel, seriously compromising operational safety [1,2]. Currently, waterproofing at shield tunnel segment joints primarily relies on elastic seal gasket systems [3]. Ethylene propylene diene monomer (EPDM) gaskets are widely used in shield tunnel waterproofing due to their excellent performance and low cost [4]. Nevertheless, under the influence of cyclic loading or combined effects from external environmental factors, these gaskets are prone to aging, misalignment, and opening, leading to a decline in sealing performance [5,6].

When waterproofing seal gaskets fail, grouting technology is typically employed for reinforcement [7]. Currently used grouting materials mainly include cement-based slurries, chemical grouts, and ultrafine mud slurries. However, these materials generally suffer from high costs, significant environmental pollution risks, poor durability, and insufficient bonding strength at the concrete interface [8–10]. Therefore, there is an urgent need to develop a new, environmentally friendly, sustainable, and highly compatible grouting waterproofing technology for tunnel joints.

Microbially induced calcium carbonate precipitation (MICP) is a biomineralization technique that utilizes microbial metabolic activity to generate calcium carbonate precipitation [11]. The core principle of this technology involves using urease-producing bacteria to decompose urea, producing carbonate ions that react with calcium ions in the environment to form calcium carbonate precipitates, thereby achieving matrix bonding, crack sealing, and impermeability reinforcement [12,13]. Compared to traditional grouting materials, MICP offers significant advantages such as environmental friendliness, chemical compatibility between reaction products and concrete matrices, and strong interfacial bonding [14]. In recent years, researchers have applied MICP technology to concrete crack repair and conducted extensive studies [15]. Relevant laboratory tests have demonstrated that MICP exhibits excellent sealing performance for concrete cracks ranging from 0.1 to 0.5 mm in width, with good interfacial adhesion between the calcium carbonate deposits and the substrate, significantly reducing the permeability coefficient of the cracks [16,17]. Additionally, by immobilizing bacteria and their nutrients within porous structures or microcapsules and incorporating them into concrete materials, self-healing microbial concrete can be developed to enable autonomous crack repair [18]. In engineering applications, Zhang et al [19]. applied formulated microbial concrete to the side walls of a lock and observed white calcite deposits forming at crack locations, effectively filling the cracks and reducing permeability. Robert Davies [20] et al. injected *Bacillus pseudomycoides* spores into lightweight perlite aggregate particles before mixing with concrete for pavement repair projects. These research findings have laid a solid theoretical and experimental foundation for applying MICP technology in waterproofing and sealing tunnel joints.

However, directly applying MICP technology to grouting and waterproofing of shield tunnel segment joints still faces significant challenges. Unlike concrete microcracks (typically less than 0.5 mm in width), the allowable gap in shield tunnel segment joints is generally 1–2 mm [21], exceeding the effective reinforcement scale achievable solely through MICP. Complete filling and effective sealing of such joints are difficult to achieve relying only on calcium carbonate precipitates generated by microbial metabolism. Furthermore, although previous studies have enhanced the efficiency and uniformity of calcium carbonate precipitation by immobilizing bacteria onto various carriers, these carriers primarily serve as supports, providing favorable attachment sites and habitats for microorganisms [22], with limited effectiveness in filling and reinforcing large-scale joints. Therefore, achieving a synergistic composite reinforcement effect between MICP technology and grouting materials—ensuring effective filling of wide joints while maintaining microbial mineralization efficiency—is a key scientific challenge in advancing the application of MICP for tunnel joint waterproofing.

Diatomite, as a natural porous siliceous material, possesses excellent properties such as high specific surface area, high porosity, and chemical stability; more importantly, diatomite is a commonly used inorganic filler material [23,24]. Diatomite particles and microbially induced calcium carbonate crystals can produce a synergistic strengthening effect, combining to seal joints. However, there has been little research on the synergistic reinforcement mechanism of diatomaceous earth combined with MICP technology for segment joints in shield tunnels.

This study employs *Bacillus pasteurii* as the microbial strain and diatomite as both a carrier and filler material to systematically investigate the enhancement of the waterproofing performance of shield tunnels. First, laboratory macro-scale tests were conducted to examine the influence of diatomite dosage on crack-sealing performance. SEM analysis was used to reveal the underlying mechanisms by which diatomite dosage enhances the waterproofing performance of tunnel joints, thereby determining the optimal dosage of diatomite. Based on this, a self-developed testing device for evaluating the waterproofing performance of shield tunnel segment joints was utilized to perform hydraulic breakdown tests on segment specimens under reinforcement by the diatomite–MICP composite grout, assessing the improvement in overall waterproofing performance of the segment joints. The research aims to enhance the overall waterproofing performance of segment joints using diatomite–MICP composite grout, providing theoretical foundations and technical references for the application of MICP technology in waterproofing shield tunnel joints, and promoting the engineering application of green biomineralization technology in underground structure waterproofing.

2. Diatomite–MICP Composite Grout Dosage Optimization Test

The principle of urease-producing microorganisms inducing calcium carbonate precipitation is shown in Figure 1, which involves the hydrolysis of urea to induce calcium carbonate precipitation. Urease-producing microorganisms decompose urea, generating CO_3^{2-}, which raises the pH of the environment. The CO_3^{2-} then reacts with Ca^{2+} in the environment to form calcium carbonate precipitate [25]. Urease-producing bacteria can be obtained from nature and are harmless to the ecological environment. The MICP reaction occurs under ambient temperature and pressure, and the raw materials used can be synergistically utilized with industrial solid waste. The calcium carbonate precipitate generated during the reaction belongs to the same calcium-based system as concrete, ensuring excellent compatibility. Therefore, MICP technology offers advantages such as environmental friendliness, strong sustainability, and high compatibility with concrete.

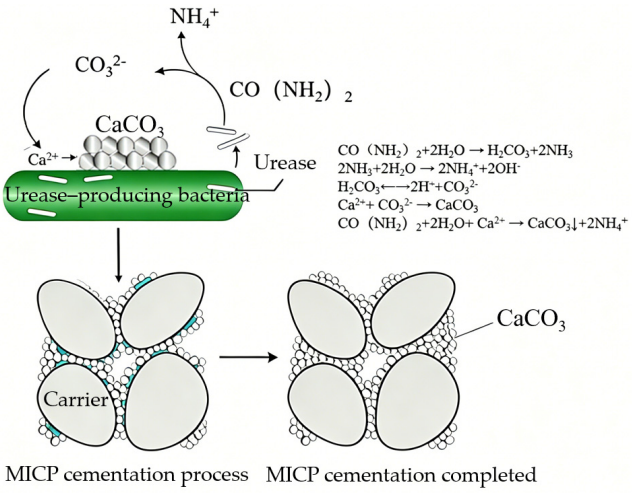

Figure 1. The urease–producing bacteria MICP process.

This study aims to use urease-producing bacteria as the MICP strain and diatomite as both a carrier and filler material. Through laboratory experimental systems, the influence of diatomite dosage on the sealing performance of diatomite–MICP composite grout for crack closure is investigated. Combined with SEM analysis, the micro-mechanism of synergistic cementation and filling of cracks by diatomite particles and calcium carbonate crystals is revealed, ultimately determining the optimal dosage of diatomite in the diatomite–MICP composite grout.

2.1. Test Materials

2.1.1. Bacterial Strains and Culture Conditions

The bacterial strain employed in this study was *Bacillus pasteurii* (ATCC 11859), obtained from an international biotechnology deposit institution, one of the strains with the strongest urease-producing ability, widely applied in MICP technology [26]. The strain was activated using a soybean casein medium composed of 5 g/L soybean peptone, 15 g/L casein peptone, and 5 g/L sodium chloride. The pH of the medium was adjusted to 7.29–7.31 with NaOH solution. After inoculating the strain into the medium, it was incubated in a constant-temperature shaking incubator at 30 °C and 130 rpm for 24 h before use. At this stage, the bacterial concentration was determined using an ultraviolet spectrophotometer with an OD600 value of 2.1 ± 0.2. Urease activity was measured using a conductivity meter, and the measured urease activity was >12.0 mM/cm·min.

2.1.2. Diatomite

The diatomite used in the experiment was a commercially available analytical-grade product with a main chemical composition of SiO_2 (content ≥ 85%) and particle size ranging from 5 to 50 μm. Diatomite is characterized by a large specific surface area and high porosity.

2.1.3. Cementing Fluid

The cementing fluid was a mixture of urea and calcium chloride, prepared using deionized water with equal amounts of urea and calcium chloride. Studies have shown that when the concentration of the cementing fluid exceeds 1 mol/L, bacterial activity is inhibited, leading to a significant decrease in calcium conversion efficiency [27,28]. Therefore, in this experiment, the concentrations of both urea and calcium chloride in the cementing fluid were set at 1.0 mol/L.

2.2. Test Methods

This study aims to prepare concrete mortar specimens with preexisting cracks, inject diatomite–MICP composite grout with varying diatomite dosage into the cracks, and investigate the influence of diatomite dosage on the crack-sealing performance through laboratory macro-scale tests. The micro-mechanism of synergistic bonding and filling by diatomite particles and calcium carbonate crystals will be revealed using SEM analysis. Ultimately, the optimal diatomite dosage in the diatomite–MICP composite grout will be determined.

2.2.1. Preparation of Concrete Specimens

Concrete mortar specimens were cast using 100 mm × 100 mm × 100 mm cubic molds. The mix proportions of the concrete mortar are presented in Table 1. Prior to casting, stainless-steel sheets with dimensions of 1 mm × 75 mm × 100 mm and 2 mm × 75 mm × 100 mm were placed at the center of the mold to prepare concrete mortar specimens with cracks of 1 mm and 2 mm, respectively [29].

Table 1. The mix proportions of the concrete mortar.

Ordinary Portland Cement (kg)	Deionized Water (kg)	Standard Sand (kg)
2	1	5.4

A release agent was applied to the surface of the steel sheets to facilitate their removal. After approximately 5 h of initial setting, the steel sheets were carefully extracted, creating cracks that spanned the top and bottom surfaces of the specimen. Subsequently, the specimens were left undisturbed for 24 h before demolding, and the demolded specimens were cured in a standard curing room. For each crack width, 63 specimens were prepared, totaling 126 specimens.

2.2.2. Preparation of Diatomite–MICP Composite Grout

Seven aliquots of the fully grown *Bacillus pasteurii* culture solution (360 mL each) were mixed with diatomite at predetermined mass ratios. Specifically, the diatomite dosages were set at 0%, 5%, 10%, 15%, 20%, 25%, and 30% of the bacterial solution, respectively. The mixtures were stirred continuously for 30 min to ensure uniform dispersion of the diatomite and sufficient adsorption of the bacterial cells. Subsequently, 7 aliquots of cementing fluid (360 mL each) were added and thoroughly mixed with the bacterial–diatomite mixtures to yield the diatomite–MICP composite grout, as shown in Figure 2.

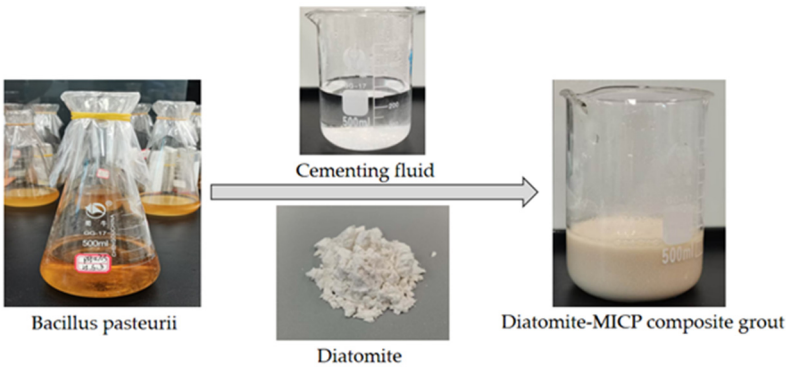

Figure 2. Preparation process of diatomite–MICP composite grout.

Finally, the composite grout was injected into the cured specimens at a rate of 5 mL/min, with three injections in total, each followed by additional injection every 8 h. After the completion of grouting, the concrete mortar specimens were cured in a standard curing room (temperature 20 ± 2 °C, relative humidity ≥ 95%) for 7 days and then removed for subsequent tests. The specimen preparation and grouting–curing process are shown in Figure 3.

2.2.3. Unconfined Compressive Strength Test

Unconfined compressive strength tests were conducted on the grouted specimens after curing. The test was performed using a YAW-2000 microcomputer-controlled electro-hydraulic servo pressure testing machine (Sansi Technology, Shanghai, China) with a strain loading rate of 0.3 mm/min. The peak stress was taken as the unconfined compressive strength of the specimen. Three parallel measurements were carried out for each test group, and the average value was adopted as the final unconfined compressive strength of the specimen.



Figure 3. Preparation and grouting process of specimens: (**a**) preparation of prefabricated crack, (**b**) curing of specimens with crack, (**c**) grouted specimens, (**d**) curing of grouted specimens.

2.2.4. Constant Normal Force Shear Test

A DJZ-500 rock direct shear testing machine (Sichuan Dexiang Company, Chengdu, China) was used to conduct constant normal load shear tests. This instrument is capable of performing both direct and dynamic shear tests, enabling the measurement of the shear mechanical properties of specimens under various conditions. After grouting and curing, the specimens were securely mounted in the apparatus with the crack surface parallel to the shear direction. A normal stress of 1.0 MPa was applied and maintained constant, followed by application of shear stress at a rate of 0.5 mm/min, during which the maximum shear stress value was recorded. Each test group consisted of three parallel measurements, and the average value was taken as the final shear strength of the specimen.

2.2.5. Falling-Head Permeability Test

The grouted and cured specimens were mounted in the permeability apparatus, as illustrated in Figure 4. The apparatus was secured using four tightening bolts to prevent lateral leakage of specimens. From top to bottom, the components are as follows:

1. Tightening bolts: Fastening bolts. The specimen and other components were secured to prevent side leakage.
2. Steel plate: Dimensions of 100 mm × 100 mm × 10 mm, featuring a central water inlet that cooperates with the tightening bolts to secure the specimen.
3. Permeable stone: Dimensions of 60 mm × 75 mm × 10 mm, embedded in a 100 mm × 100 mm × 15 mm silicone rubber matrix. It serves to buffer water flow and ensure uniform permeation. Additionally, rubber is bonded to the bottom edges of the silicone rubber. The elastic rubber conforms to the surfaces of the steel plate and specimen, preventing lateral leakage during testing.
4. Iron stand: Supports the permeability apparatus to maintain stability.
5. Water collection container: Positioned at the base of the apparatus to collect permeated water.

During testing, the initial water head height was set at 100 cm. The water head height was recorded after 10 min. Three parallel determinations were conducted for each group, and the permeability coefficient was calculated using the falling-head permeability formula. The average value was adopted as the final permeability coefficient of the specimen.

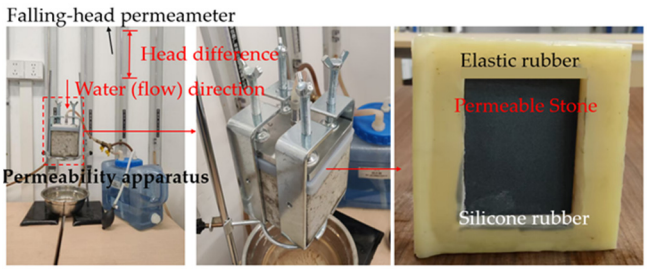

Figure 4. Schematic diagram of the falling-head permeability test apparatus.

The diatomite–MICP dosage optimization test scheme is shown in Table 2 below.

Table 2. Test schemes for concrete specimens.

Diatomite Dosage	Use of Specimens					
	Unconfined Compressive Strength Test		Constant Normal Force Shear Test		Falling-Head Permeability Test	
	1 mm Crack	2 mm Crack	1 mm Crack	2 mm Crack	1 mm Crack	2 mm Crack
0	3	3	3	3	3	3
5%	3	3	3	3	3	3
10%	3	3	3	3	3	3
15%	3	3	3	3	3	3
20%	3	3	3	3	3	3
25%	3	3	3	3	3	3
30%	3	3	3	3	3	3

2.2.6. Microstructure Study

To gain a deeper understanding of the crack-sealing mechanism of diatomite–MICP composite grout, the micro-morphology of the composite grout after drying was observed using an Axia Chemi SEM (Thermo Fisher Scientific, Brno, Czech Republic). The samples were gold-coated and placed on the scanning electron microscope sample stage for morphological analysis.

The process of the diatomite–MICP composite grout dosage optimization test is shown in Figure 5.

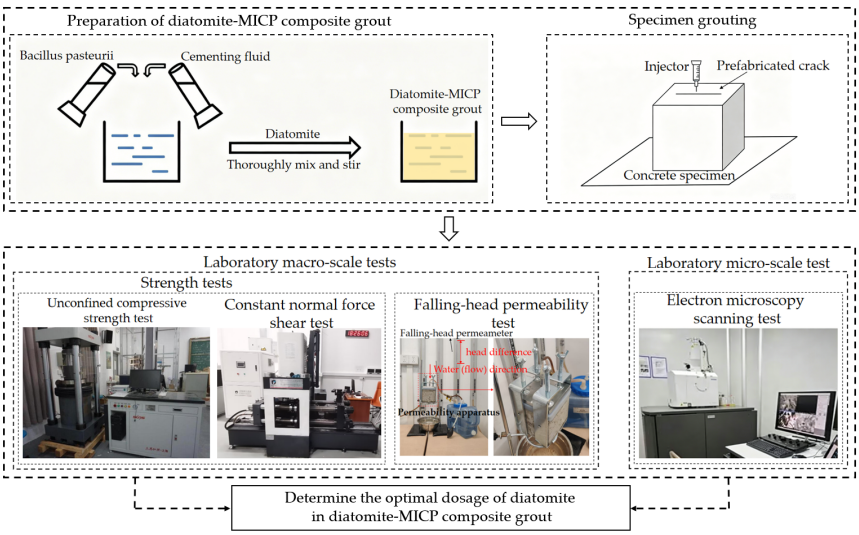

Figure 5. Schematic diagram of the test process.

3. Results of the Diatomite–MICP Composite Grout Dosage Optimization Test

3.1. Analysis of Laboratory Strength Tests

Figure 6 presents the unconfined compressive strength test results of specimens under different treatment conditions. For the 1 mm crack specimens, the unconfined compressive strength of the group without diatomite was 21.40 MPa, with a shear strength of 3.23 MPa. After grouting with composite grout containing 20% diatomite, the specimens achieved the highest unconfined compressive strength and shear strength, reaching 23.65 MPa and 3.54 MPa, respectively—representing increases of 10.51% and 9.60% compared to the group without diatomite (0%). In the 2 mm crack specimens, the specimens with 20% diatomite achieved the maximum strengths of 18.98 MPa in unconfined compressive strength and 3.36 MPa in shear strength, representing increases of 13.99% and 9.45%, respectively, compared to the group without diatomite.

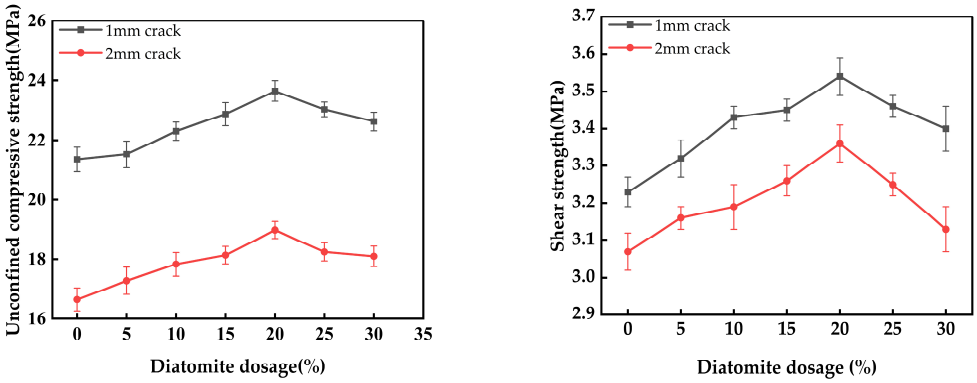

(**a**) (**b**)

Figure 6. Laboratory strength test results. (**a**) Unconfined compressive strength results, (**b**) shear strength results.

The repair performance of diatomite–MICP composite grout was superior to that of the control group without diatomite, with the best results achieved when the diatomite dosage was 20%. This is primarily because the addition of an appropriate amount of diatomite enables bacteria adsorbed on the surface of diatom particles to form a dense layer of calcium carbonate crystal precipitates on crack walls. The gaps between diatom particles are also filled with calcium carbonate, creating a diatomite–calcium carbonate composite bonding system that thoroughly fills the cracks. When the diatomite dosage is less than 20%, insufficient nucleation sites for calcium carbonate crystals lead to easy bacterial loss, preventing the diatomite–MICP composite grout from fully filling the cracks. When the diatomite dosage exceeds 20%, the fluidity of the composite grout decreases. Since diatomite itself has much lower strength than calcium carbonate crystals, excessive diatom particles can result in locally weak filling, causing a declining trend in both unconfined compressive strength and shear strength.

3.2. Analysis of Permeability Coefficient

Figure 7 shows the experimental results of permeability coefficient for 1 mm and 2 mm crack specimens under different diatomite dosage conditions. As the diatomite dosage increased, the permeability coefficient initially decreased and then increased. When the diatomite dosage reached 20%, the permeability coefficient dropped to its minimum value of 3.48×10^{-4} cm/s, representing a reduction of 69.97% compared to the group without diatomite (0%). However, further increasing the diatomite dosage to 25% and 30% caused the permeability coefficient to rise again to 4.13×10^{-4} cm/s and 4.43×10^{-4} cm/s, respec-

tively. The 2 mm crack specimens exhibited a similar trend: the permeability coefficient for the group without diatomite was 2.93 × 10^{-3} cm/s, while at a diatomite dosage of 20%, it reached its lowest value of 1.03 × 10^{-3} cm/s, indicating a reduction of 64.84% compared to the control group (0%).

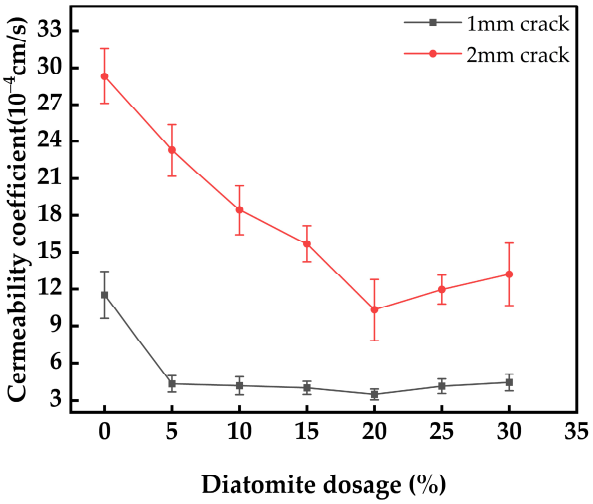

Figure 7. Results of the falling-head permeability test.

Based on the above results, when the diatomite dosage is low, its porous structure provides an excellent attachment substrate for *Bacillus pasteurii*, increasing bacterial retention within cracks. Consequently, as the diatomite dosage increases, the amount of calcium carbonate precipitation rises and its distribution becomes more uniform, gradually enhancing crack-sealing performance. However, when the diatomite dosage exceeds 20%, the accumulated pores between diatomite particles increase overall permeability, preventing calcium carbonate crystals from fully filling the cracks between diatomite particles, thereby reducing waterproofing effectiveness and increasing the permeability coefficient.

3.3. Analysis of Microscopic Mechanism

Figure 8 showed SEM images of the dried diatomite–MICP composite grout with diatomite dosage of 15%, 20%, and 25%. When the diatomite dosage was 15%, the density of nucleation sites on the surface of the diatomite particles was relatively low. Due to insufficient nucleation sites for calcium carbonate crystals, some crystals formed as large, irregularly shaped bodies in free space. These crystals could not pack closely together, leaving numerous pores. When the diatomite dosage increased to 20%, the density of nucleation sites became optimal. The silanol groups on the surface of the diatomite particles provided enough adsorption sites for calcium ions, allowing calcium carbonate crystals to distribute uniformly on the diatomite surface. The calcium carbonate crystals completely encapsulated the diatomite particles, forming a dense composite bonding matrix consisting of diatomite particles and calcium carbonate crystals. However, when the diatomite dosage was further increased to 25%, although the nucleation site density was high, the excessive diatomite particles negatively affected the MICP reaction: they occupied too much space, restricting calcium ions to form only small-sized crystals within limited areas. These small calcium carbonate crystals failed to adequately fill the pores between the excessive diatomite particles, significantly reducing the compactness of the composite bonding matrix.



(**a**) (**b**) (**c**)

Figure 8. SEM images of diatomite–MICP composite grout at different diatomite dosage: (**a**) 15% diatomite dosage, (**b**) 20% diatomite dosage, (**c**) 25% diatomite dosage.

3.4. Analysis of the Optimal Dosage of Diatomite

The dosage of diatomite significantly affects the crack-sealing performance of diatomite–MICP composite grout. When the diatomite dosage is 20%, the sealing effect was optimal. Both 1 mm and 2 mm crack specimens showed reduced permeability coefficients and improved unconfined compressive strength and shear strength. However, when the diatomite dosage exceeds or falls below 20%, the sealing effectiveness decreases. Microscopic mechanism analysis indicated that when the diatomite dosage was less than 20%, the grout could not fully fill the cracks. Conversely, when the dosage exceeded 20%, the fluidity of the grout decreased, and excessive accumulation of diatomite particles creates additional pores, increasing overall permeability. As a result, calcium carbonate crystals failed to completely fill the cracks between diatomite particles, leading to reduced sealing efficiency.

Considering the mechanical tests, the reduction in permeability, and the injectability of the grout, the optimal dosage of diatomite was determined to be 20% by mass of the bacterial solution, providing a theoretical basis for preparing diatomite–MICP composite grout in the subsequent water pressure tests.

4. Water Pressure Test for Segment Joint with Diatomite–MICP Grouting Reinforcement

Based on the above optimization tests, it was determined that a 20% diatomite dosage in the diatomite–MICP composite grout achieved the highest improvement in overall performance and best waterproofing capability when reinforcing 1–2 mm cracks. To investigate the waterproofing enhancement of the 20% diatomite-containing composite grout in actual shield tunnel segments, a water pressure breakdown test for segment joints with the composite grout was designed.

4.1. Test Equipment

The waterproofing of shield tunnel segment joints primarily relies on an elastic seal gasket system. During segment assembly, axial compressive force is applied to maintain the compression of the gaskets, thereby preventing external water from penetrating. This study has designed a water pressure test platform, integrating axial drive, reaction support, positioning locking, lifting assistance, water injection, and water pressure measurement. As shown in Figure 9, the platform consists of the following components:

1. Jack. The test platform employs a bidirectional hydraulic short-stroke jack to provide horizontal thrust, with a rated output force of up to 20 tons, controlled by an oil pump.
2. Reaction frame. To withstand the axial reaction force generated by the jack and the hydrostatic pressure, a reaction frame was designed and developed for this test. Based

on mechanical calculations, the structural design capacity of the frame is set at 45 tons, ensuring structural reliability during testing.

3. Limiting device. This device consists of four sets of high-strength limiting threaded rods, along with matching pressure sensors and nut assemblies, arranged in a rectangular pattern at the four corners of the reaction frame. Each rod has a maximum tensile strength of up to 25 tons, effectively handling the reaction forces caused by seal gaskets under various joint configurations and water pressure.
4. Bull's eye wheel. The wheel was used to restrict and adjust the front-to-back positions of two segments, aligning the seal gaskets and minimizing testing errors.
5. Manual hoist. A manual hoist is installed above the test platform to lift, assemble, and disassemble the segments.
6. Water tank. A water tank is placed beneath the test platform to collect leakage water from the segment joints.
7. Water injection system. A single pump is adopted, operating in constant flow mode with an injection rate of 25 mL/min.
8. Data acquisition system. Pressure sensors are used to monitor water pressure, and data are collected with a micro-strain data acquisition system.
9. Software control center. A computer must be connected to acquire data with the corresponding software.

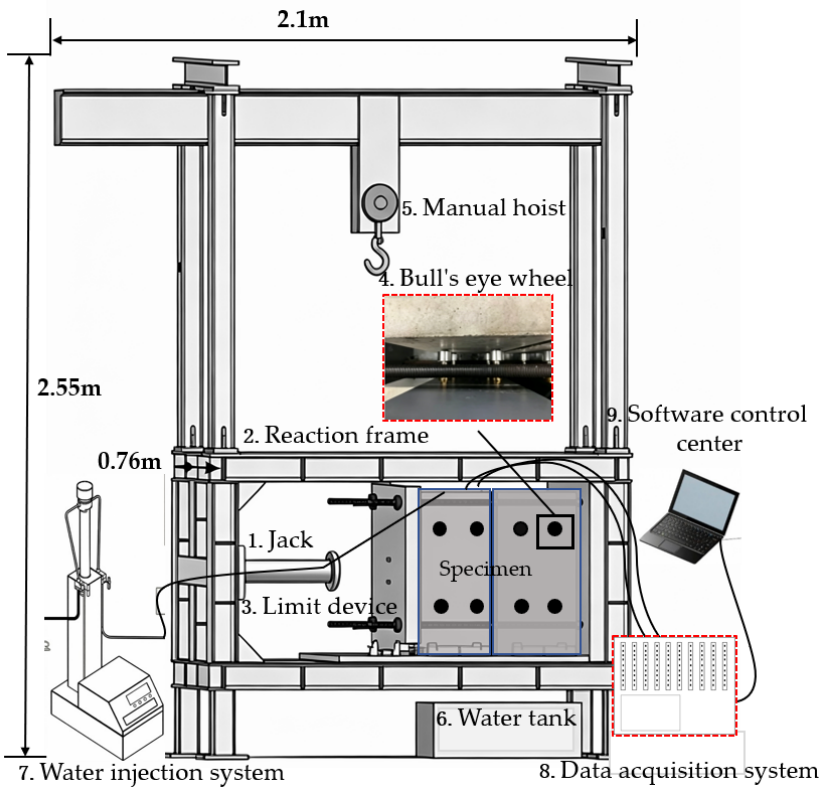

Figure 9. Overall schematic diagram of the test platform.

4.2. Test Methods

4.2.1. Specimen Preparation

As the burial depth and diameter of shield tunnels continue to increase, the surrounding environment becomes increasingly complex, thereby raising the requirements for waterproofing performance at tunnel segment joints. Consequently, an increasing number of large-diameter shield tunnels crossing rivers and seas now employ double-seal gaskets to prevent joint leakage. Under identical conditions, double-seal gaskets offer superior waterproofing capability compared to single-seal gaskets [30]. As shown in Figure 10, water

first enters the external seal cavity and is blocked by the outer seal gasket. If the water pressure overcomes the outer seal gasket, it then flows into the internal seal cavity. When the water pressure reaches the breakdown threshold of the inner seal gasket, the inner seal gasket fails, rendering the entire waterproofing system ineffective and causing leakage in the tunnel.

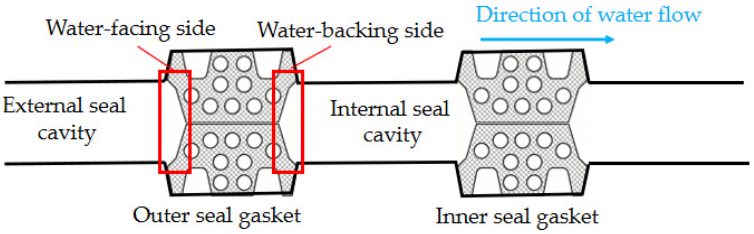

Figure 10. Schematic diagram of waterproofing with double-seal gasket.

The height of the specimen was selected as 600 mm, matching the standard thickness commonly used for tunnel segments in engineering practice. This ensures geometric similarity between the specimen and actual structures, while also providing sufficient space for the proper arrangement of a dual-seal gasket. The specimen's length and width were chosen as 300 mm and 350 mm, respectively, ensuring that the effective length of the seal gasket meets experimental requirements and allows full demonstration of its mechanical and waterproofing performance during compression. Auxiliary seal gaskets are applied around the perimeter of the specimen to ensure tight sealing. These auxiliary gaskets are made of the same material as the outer and inner seal gaskets but feature shallower grooves, enabling greater compression under horizontal pressure and thus enhancing waterproofing capacity. C50-grade concrete was selected for the concrete specimens. Additionally, six stainless-steel pipes were embedded into each specimen during casting, serving purposes such as water injection, grouting, air venting, and monitoring the water pressure in both internal and external seal cavities. The structural design model of the specimen is shown in Figure 11.

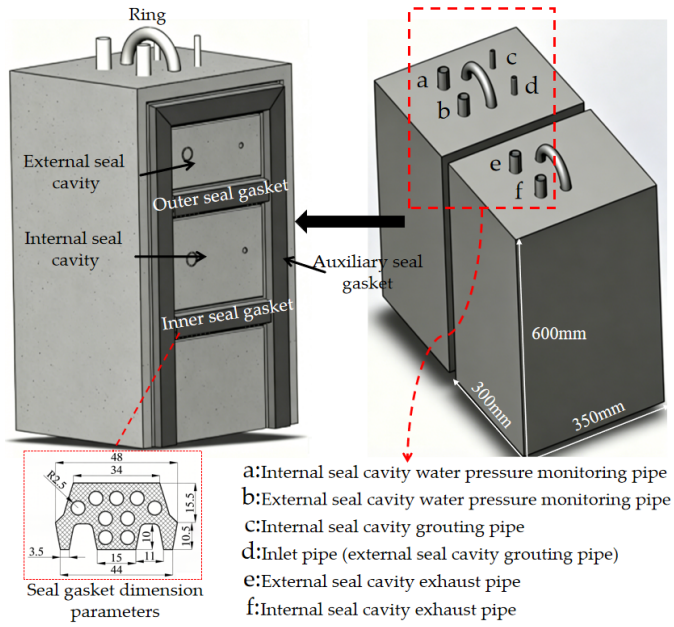

Figure 11. Model of specimen structure design.

The waterproof seal gasket is made of porous ethylene propylene diene monomer (EPDM) rubber, the most widely used material in shield tunnel joints. The dimensional

parameters of the gasket are shown in Figure 11. The material properties of the EPDM gasket are listed in Table 3.

Table 3. Parameters of EPDM seal gasket materials.

Performance Items	Performance Metrics
Hardness (SH, degree)	65 ± 5
Elongation at break (%)	≥330
Tensile strength (MPa)	≥10
Hardness change value (SH)	≤6
Thermal air aging (70 °C × 96 h) tensile strength change rate (%)	≤15
Elongation at break rate (%)	≤30
Compression set (%) (23 °C × 72 h, 25%)	≤15
Compression set (%) (70 °C × 24 h, 25%)	≤25
Mold resistance grade	Grade 1

4.2.2. Gasket Breakdown Hydrostatic Test Without Grouting

To evaluate the waterproofing performance of the seal gasket used in this test and compare it with the waterproof effect after grouting reinforcement, specimens were prepared and cured and then subjected to a water pressure test for seal gasket breakdown under non-grouted conditions. Before commencing the test, the integrated waterproofing performance testing system for segment joints was assembled as shown in Figure 9. After completing the setup, the preparation phase began. First, the specimen was lifted and positioned using a manual hoist, and its front and back alignment were fine-tuned with a bull's-eye wheel. Then, water supply and exhaust pipes, along with water pressure monitoring sensors, were connected. Finally, a hydraulic jack was used to push the specimen to control the joint width, while nuts on the limit rod rigidly constrained the joint width, as illustrated in Figure 12. In accordance with the applicable specification [31], the maximum allowable joint opening during construction must not exceed 6 mm. This limit ensures that the sealing system has sufficient compression capacity. Therefore, in this test, the joint opening was designed to be 6 mm.



Figure 12. Test preparation process: (**a**) specimen hoisting, (**b**) specimen joint width control, (**c**) connection of water injection, exhaust pipe, and water pressure monitoring sensor.

After the preparation phase was completed, the water pressure test began. First, the signal lines of the water pressure monitoring sensors were connected to the micro-strain data acquisition instrument. Then, an ISCO pump (Teledyne ISCO, Lincoln, NE, USA) was used to fill water and purge air from the external seal cavity. When water flowed continuously out from the external seal cavity's exhaust pipe, it indicated that all air had been expelled from the external seal cavity. Subsequently, the external seal cavity exhaust valve was immediately closed, and water continued to be injected into the external seal cavity under sustained pressure while changes in the water pressure sensor readings were closely monitored. When the outer seal gasket was broken, a sudden drop in pressure appeared on the pressure–time curve, and the peak pressure value at this point represents the breakdown water pressure of the outer seal gasket. After the outer seal gasket was breached, water flowed into the internal seal cavity. Continuing water injection and observing the outlet of the internal seal cavity's exhaust pipe, when water started flowing out, it indicated that the internal seal cavity was fully filled with water and all air had been removed. At this point, the internal seal cavity exhaust valve was closed and pressurizing the seal cavity using the water injection system continued. When leakage occurred at the joint, a sharp drop in the pressure–time curve of the internal seal cavity indicated that the inner seal gasket had been breached, resulting in overall failure of the joint waterproofing system. The recorded pressure value at this moment was defined as the breakdown water pressure of the inner seal gasket. The water pressure loading process is illustrated in Figure 13.

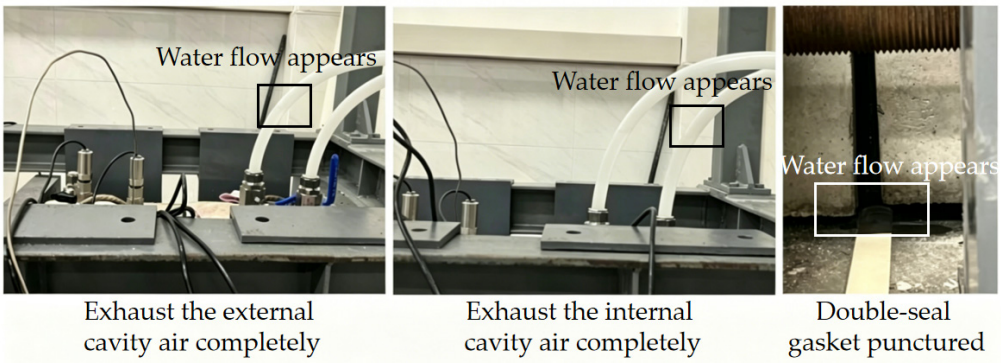

Figure 13. Water pressure loading process.

4.2.3. Gasket Breakdown Test with Diatomite–MICP Composite Grout

After the test under the ungrouted condition, a new test was conducted under the MICP-gasket composite grouting condition. Based on the optimal dosage ratio determined from the previous tests, the diatomite–MICP composite grout was prepared and injected separately into the internal seal cavity and external seal cavity through the grouting pipes. When grout appeared at the exhaust pipes of both cavities, the grouting was considered complete, as shown in Figure 14. Subsequently, the specimen was cured at room temperature for 21 days. After curing, the gasket breakdown test was performed. The test procedure was essentially the same as that of the ungrouted-condition test.

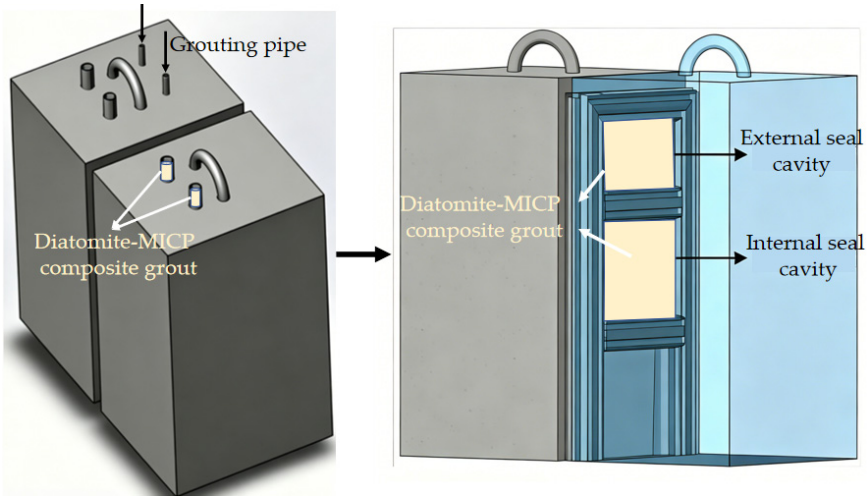

Figure 14. Schematic diagram of specimen grouting.

5. Results of Gasket Breakdown Test

Figure 15 shows the variation in water pressure in the internal seal cavity and external seal cavity during the test under diatomite–MICP grouting conditions compared to the test without grouting. In the ungrouted-condition test, water was injected into the external seal cavity through the inlet pipe. Once the external seal cavity was fully filled with water, the external seal cavity pressure sensor began recording pressure data, and the cavity pressure gradually increased. When the pressure reached the breakdown point of the outer seal gasket, the gasket failed, causing a sharp drop in the external seal cavity pressure. After the outer seal gasket broke through, water flowed into the internal seal cavity. Once the internal seal cavity was completely filled, the cavity pressure sensor started detecting pressure data. At this point, the pressures in both cavities began rising synchronously in a stepwise manner. When the pressure reached the breakdown level of the inner seal gasket, the inner seal gasket failed, resulting in a rapid decline in pressure in both cavities.

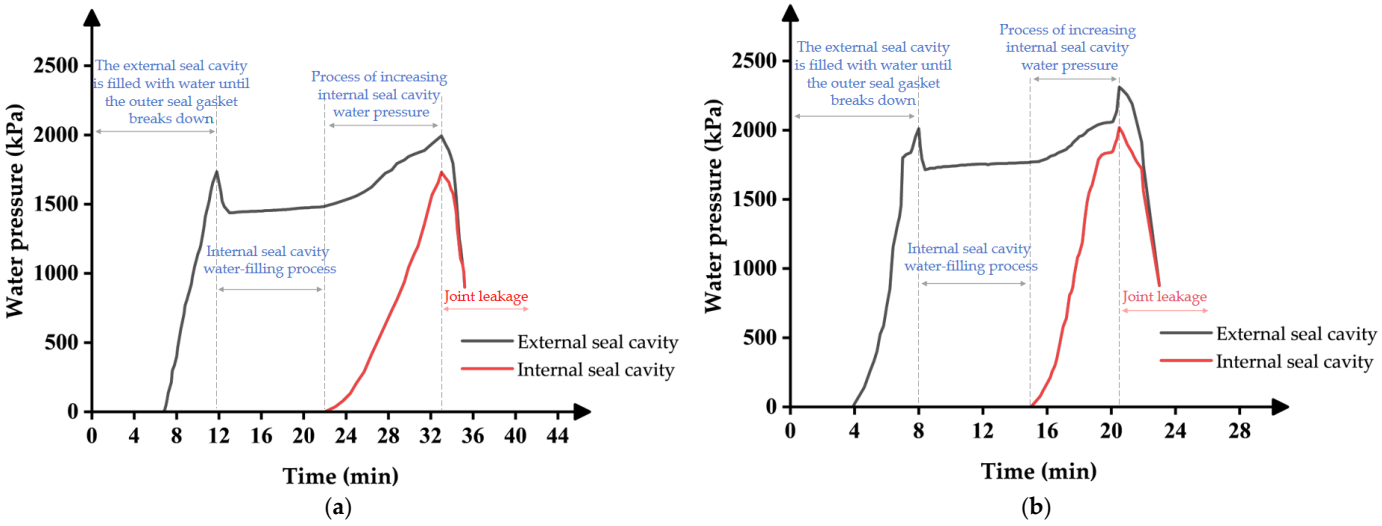

Figure 15. Breakdown hydraulic test results. (**a**) Ungrouted condition. (**b**) Grouted condition.

As shown in Figure 15, the external seal cavity water pressure measured at the inner seal gasket breakdown was higher than that measured at the outer seal gasket breakdown. This is because when the outer seal gasket is breached, water flows into the internal seal cavity. As the inner cavity fills with water, the water-backing side of the outer seal

gasket is subjected to water pressure from within. Consequently, the outer seal gasket changes from being under pressure on the water-facing side only to being compressed on both sides, increasing the local contact stress and thereby enhancing its waterproofing performance. In grouting condition tests, the rate of increase in water pressure within both cavities was faster compared to non-grouting conditions. This is because after the diatomite–MICP composite grout filled the joint, both cavities were largely occupied by a diatomite–calcium carbonate composite binder, allowing water to quickly fill the remaining space. Additionally, after adding the composite grout, when the inner seal gasket and outer seal gasket were breached, the water pressure initially rose slowly before increasing rapidly. This phenomenon results from water first penetrating through the composite binder formed by diatomite particles and calcium carbonate crystals.

Under non-grouting conditions, the water pressure at which the outer seal gasket failed was 1735 kPa, while that for the inner seal gasket was 1731 kPa, indicating that the waterproofing performance of both gaskets was nearly equivalent. In the test group treated with diatomite–MICP composite grout, the failure water pressure of the outer seal gasket reached 2011 kPa and that of the inner seal gasket reached 2019 kPa, representing increases of 15.91% and 16.64%, respectively, compared to the control group.

The improvement in breakdown water pressure can be explained from two aspects. First, the diatomite–calcium carbonate composite binder within the joint fills the micro-gaps between the EPDM seal gasket and the concrete groove. The deposition of calcium carbonate crystals enhances the contact tightness between the seal gasket and the groove wall, effectively improving the compression sealing efficiency of the seal gasket. Second, as external water pressure gradually increases, the incorporation of diatomite particles promotes more uniform and dense calcium carbonate precipitation. The composite binder consisting of diatomite particles and calcium carbonate crystals fully fills the joint cavity, providing additional waterproofing effects and further enhancing the overall waterproofing performance of the waterproofing system.

6. Discussion

Compared with traditional grouting materials, diatomite–MICP composite grouting technology exhibits distinct advantages. Traditional cement-based slurries are prone to interfacial bonding failure due to shrinkage and struggle to fill micro-cracks, while chemical grouts face risks of environmental pollution and aging degradation. In contrast, the calcium carbonate precipitates generated by MICP exhibit excellent compatibility with the concrete matrix, while the physical filling effect of diatomite effectively seals wide joints. However, the biomineralization process is constrained by bacterial activity, resulting in slower curing rates [32] and lower instant sealing efficiency compared to polyurethane and other chemical grouts, which limits its application in emergency rescue scenarios. In terms of economic feasibility, the price of diatomite is approximately 1800–4000 RMB/ton, which is significantly lower than traditional polyurethane and epoxy resins (12,000–17,000 RMB/ton). Although bacterial cultivation adds cost, various methods are currently being employed to substantially reduce its price [33]. More importantly, the excellent sustainability of this technology can significantly reduce repeated treatment costs during the operation period, yielding significant full lifecycle cost-effectiveness benefits [34]. It is particularly suitable for the refined treatment of micro-leakages in shield tunnel joints and environmentally sensitive areas.

The use of stainless-steel sheets to prefabricate cracks in the optimization phase was intended to simplify the quantitative evaluation of dosage, while the subsequent phase employed a large-scale joint model with realistic dimensions. Nevertheless, these models cannot fully replicate the complex geological and loading conditions of actual

tunnel engineering. Furthermore, the current understanding of micro-mechanisms relies primarily on morphological observations from SEM, lacking quantitative data on crystal phase composition or chemical bonding. Future studies should incorporate complementary techniques like XRD or TGA.

It should be noted that the current laboratory tests were conducted using simplified specimens under controlled conditions. In actual shield tunnel environments, segment joints are significantly influenced by complex coupled conditions, including non-uniform earth pressure, seepage, temperature fluctuations, and dynamic loads induced by operation or adjacent construction [35]. These complex in situ conditions may adversely affect the stability and effectiveness of the diatomite–MICP composite grout. This implies that existing laboratory test results may overestimate the enhancement in waterproofing performance of the composite grout under actual field conditions. Therefore, future research will focus on investigating the long-term durability of the diatomite–MICP composite grout within the complex environment of actual shield tunnels, aiming to evaluate its long-term performance under real-world complex coupled conditions.

7. Conclusions

This study investigates the influence of diatomite dosage on the crack-sealing performance of diatomite–MICP composite grout through laboratory experimental systems. After that, with a self-developed testing device, water pressure breakdown tests were conducted on segment specimens under reinforcement by the diatomite–MICP composite grout, systematically assessing the improvement in overall waterproofing performance of segment joints. Based on these test results, the following conclusions can be drawn:

1. The dosage of diatomite significantly affects the crack-sealing performance of the diatomite–MICP composite grout. When the diatomite dosage is 20%, the composite grout achieves optimal sealing performance, showing identical effects on both 1 mm and 2 mm crack specimens—namely, reduced permeability coefficient and increased unconfined compressive strength and shear strength. However, when the diatomite dosage is either insufficient or exceeds 20%, the sealing effectiveness of the composite grout decreases. Therefore, a diatomite dosage of 20% of the bacterial solution mass provides the best overall improvement.
2. When the diatomite dosage is 20%, the diatomite particles provide sufficient living space and a favorable environment for *Bacillus pasteurii*. The silanol groups on the surface of diatomite offer abundant adsorption sites for calcium ions, enabling uniform distribution of calcium carbonate crystals on the diatomite surface until they completely encapsulate the particles, forming a dense composite binder consisting of diatomite particles and calcium carbonate crystals. When the diatomite dosage is insufficient or exceeds 20%, the composite binder shows a decrease in density.
3. The joint water pressure test verified the effectiveness of diatomite–MICP composite grout in tunnel joint waterproofing. With a joint opening of 6 mm, the breakdown water pressures for the inner and outer seal gaskets at the segment joints injected with optimized diatomite–MICP composite grout reached 2011 kPa and 2019 kPa, respectively—representing increases of 15.91% and 16.64% compared to the control group without grouting. A synergistic waterproofing effect was achieved between the diatomite–MICP composite grout and the EPDM seal gasket, as the composite bonding material filled micro-cracks between the segment joints and the interface between the seal gasket and concrete groove, thereby enhancing the overall waterproofing performance of the sealing system.

The research results indicate that the combination of diatomite and MICP reinforcement technology enhances the overall waterproofing performance of tunnel joints by

effectively filling wide joints and reinforcing the seal gasket system. Future research will focus on the long-term durability of diatomite–MICP composite grout in complex engineering environments, as well as the optimization of field grouting operations and parameters, to promote the practical application of MICP technology in tunnel engineering.

Author Contributions: Conceptualization: C.L., X.N. and Y.L.; methodology: C.L. and Y.L.; validation: X.N. and Y.L.; formal analysis: C.L.; investigation: C.L. and Q.Y.; resources: X.N. and Q.Y.; data curation: C.L.; writing—original draft preparation: Y.L. and C.L.; writing—review and editing: Y.L. and X.N.; visualization: C.L.; supervision: X.N. and Y.L.; project administration: X.N. and Q.Y.; funding acquisition: Y.L. All authors have read and agreed to the published version of the manuscript.

Funding: This work is supported by the National Key R&D Program of China (No.2024YFC3809002), the National Natural Science Foundation of China (No. 52378427), and the Guangdong Basic and Applied Basic Research Foundation (No. 2024A1515012623).

Institutional Review Board Statement: Not applicable.

Informed Consent Statement: Not applicable.

Data Availability Statement: The original contributions presented in this study are included in the article. Further inquiries can be directed to the corresponding author.

Conflicts of Interest: Authors Xingzhong Nong and Quan Yuan was employed by the company Guangzhou Metro Design & Research Institute Co., Ltd. The remaining authors declare that the research was conducted in the absence of any commercial or financial relationships that could be construed as a potential conflict of interest.

References

1. Gong, C.; Wang, Y.; Ding, W.; Lei, M.; Shi, C. Waterproof performance of sealing gasket in shield tunnel: A review. *Appl. Sci.* **2022**, *12*, 4556. [CrossRef]
2. Zhang, D.-M.; Liu, J.; Huang, Z.-K.; Yang, G.-H.; Jiang, Y.; Jia, K. Waterproof performance of tunnel segmental joints under different deformation conditions. *Tunn. Undergr. Space Technol.* **2022**, *123*, 104437. [CrossRef]
3. Xiao, M.; Xie, H.; Wang, S.; Zhong, Y. Evolution and prospects of shield tunnel joints and segment waterproofing systems. *Tunn. Constr.* **2021**, *41*, 1891–1902. [CrossRef]
4. Wang, X.; Hou, D.; Li, S. Study on the Seepage Mechanism of Gaskets at the Joints of Shield Segments Based on Coupled Euler-Lagrangian Method. *Water* **2024**, *16*, 1661. [CrossRef]
5. Hu, Z.; Zhang, C.; Meng, S.; Du, Y.; Ma, K.; Wang, H.; Qie, B.; Xu, S. Encapsulated anti-aging approach on rubber sealing gasket of shield tunnel segment joint: A multiscale comparative experimental study. *Tunn. Undergr. Space Technol.* **2025**, *164*, 106854. [CrossRef]
6. Li, H.-Y.; Wu, H.-N.; Cao, H.; Chen, R.-P. Long-term waterproof performance of EPDM sealing gaskets considering aging-induced stress relaxation. *Tunn. Undergr. Space Technol.* **2026**, *168*, 107117. [CrossRef]
7. Li, D.; Jiang, Y. Study on the Leakage Cause and Treatment Technology of Underwater Shield Tunnel During Operation Period. *China Build. Waterproofing* **2020**, *10*, 14–17.
8. Ji, X.; Dong, L.; Li, X.; Lu, H.; Song, H.; Wen, P. Green Grouting Material Based on Phosphogypsum–Slag Geopolymer: Feasibility and Performance Evaluation for Trenchless Road Repair. *Materials* **2025**, *18*, 4901. [CrossRef] [PubMed]
9. Qian, Z.; Zheng, H.; Jiang, C.; Zhang, G. Experimental study on patterns and mechanisms of water quality degradation in water-rich sand formations induced by different types of chemical grouts. *J. Contam. Hydrol.* **2026**, *281*, 104947. [CrossRef] [PubMed]
10. Zhou, J.; Zha, L.; Meng, S.; Zhang, Y. Optimization on overall performance of Modified Ultrafine Cementitious Grout Materials (MUCG) and hydration mechanism analysis. *PLoS ONE* **2024**, *19*, e0309312. [CrossRef] [PubMed]
11. Zhu, J.; Wei, R.; Peng, J.; Dai, D. Improvement schemes for bacteria in MICP: A review. *Materials* **2024**, *17*, 5420. [CrossRef] [PubMed]
12. Wang, J.; Ji, S.; Huang, S.; Jiang, Z.; Wang, S.; Zhang, H.; Wang, Z.; Zhang, J. Crack sealing in concrete with biogrout: Sustainable approach to enhancing mechanical strength and water resistance. *Materials* **2024**, *17*, 6283. [CrossRef] [PubMed]
13. Zhou, G.; Fang, X.; Shen, C.; Chen, Z.; Bao, T.; Yao, Z. Shaking table test for microbial coral sand pile composite foundations and coral sand foundations. *Earthq. Eng. Eng. Vib.* **2026**, *25*, 379–391. [CrossRef]

14. Omoregie, A.I.; Wong, C.S.; Rajasekar, A.; Ling, J.H.; Laiche, A.B.; Basri, H.F.; Sivakumar, G.; Ouahbi, T. Bio-based solutions for concrete infrastructure: A review of microbial-induced carbonate precipitation in crack healing. *Buildings* **2025**, *15*, 1052. [CrossRef]
15. Wang, J.; Li, Y.; Zhang, S.; Zhang, H.; Li, Z. Decoupling of permeability and strength recovery in microbial-induced calcium carbonate precipitation (MICP) for concrete crack repair. *Results Eng.* **2026**, *29*, 109910. [CrossRef]
16. Zhang, Y.; Liu, Y.; Sun, X.; Zeng, W.; Xing, H.; Lin, J.; Kang, S.; Yu, L. Application of microbially induced calcium carbonate precipitation (MICP) technique in concrete crack repair: A review. *Constr. Build. Mater.* **2024**, *411*, 134313.
17. Wong, P.Y.; Mal, J.; Sandak, A.; Luo, L.; Jian, J.; Pradhan, N. Advances in microbial self-healing concrete: A critical review of mechanisms, developments, and future directions. *Sci. Total Environ.* **2024**, *947*, 174553. [CrossRef] [PubMed]
18. Ma, W.; Sun, D.; Ma, X.; Cui, S. Preparation and investigation of self-healing cementitious composite based on DMTDA-epoxy binary microcapsules system. *J. Build. Eng.* **2022**, *56*, 104779. [CrossRef]
19. Zhang, X.; Qian, C. Engineering application of microbial self-healing concrete in lock channel wall. *Mar. Georesour. Geotechnol.* **2022**, *40*, 96–103.
20. Davies, R.; Teall, O.; Pilegis, M.; Kanellopoulos, A.; Sharma, T.; Jefferson, A.; Gardner, D.; Al-Tabbaa, A.; Paine, K.; Lark, R. Large scale application of self-healing concrete: Design, construction, and testing. *Front. Mater.* **2018**, *5*, 51. [CrossRef]
21. *GB 50446-2017*; Code for Construction and Acceptance of Shield Tunnelling Method. China Planning Press: Beijing, China, 2017.
22. Lu, W.; Hu, S.; Wang, Y.; Jiang, L. Review on the Influence of Carrier Materials on the Self-healing Effect of Microbial. *J. Mater. Sci. Eng.* **2024**, *42*, 680–691.
23. Kipsanai, J.J.; Wambua, P.M.; Namango, S.S.; Amziane, S. A review on the incorporation of diatomaceous earth as a geopolymer-based concrete building resource. *Materials* **2022**, *15*, 7130. [CrossRef] [PubMed]
24. Alex, A.G.; Jose, P.A.; Saberian, M.; Li, J. Green pervious concrete containing diatomaceous earth as supplementary cementitous materials for pavement applications. *Materials* **2022**, *16*, 48. [CrossRef] [PubMed]
25. Nobari, A.Z.; Jabbarzadeh, M.; Bertola, N.; Sengupta, A.; Lavasan, A.A. Sustainable bio-based construction: A review of MICP technology and bio-cementation across scales and materials. *Case Stud. Constr. Mater.* **2026**, *24*, e06100. [CrossRef]
26. Khoshtinat, S. Advancements in exploiting sporosarcina pasteurii as sustainable construction material: A review. *Sustainability* **2023**, *15*, 13869. [CrossRef]
27. Lai, H.-J.; Cui, M.-J.; Wu, S.-F.; Yang, Y.; Chu, J. Retarding effect of concentration of cementation solution on biocementation of soil. *Acta Geotech.* **2021**, *16*, 1457–1472. [CrossRef]
28. Tao, H.; Sun, C.; Qu, J.; Huang, Y. Study on the effect of cementation solution concentration on sand fixation by fiber reinforced MICP. *PLoS ONE* **2025**, *20*, e0329673. [CrossRef] [PubMed]
29. Li, G.; Yan, D.; Liu, J.; Yang, P.; Zhang, J. Study on the mechanical properties of crack mortar repaired by enzyme-induced calcium carbonate precipitation (EICP). *Materials* **2024**, *17*, 2978. [CrossRef] [PubMed]
30. Ding, W.; Wang, Q.; Qiao, Y.; Jin, Y. Experimental investigation on waterproofing performance of segmental joint with double gaskets for shield tunnel. *Undergr. Space* **2022**, *7*, 898–910. [CrossRef]
31. *GB 50108-2008*; Technical Code for Waterproofing of Underground Works. China Planning Press: Beijing, China, 2008.
32. Wei, R.; Peng, J.; Xu, P.; Li, L. Influence of aluminum ion flocculants on the effect of MICP reinforcement of sand. *J. Civ. Environ. Eng.* **2025**, *47*, 71–79.
33. Yan, Z.; Nakashima, K.; Takano, C.; Kawasaki, S. Strategies for cost-optimized biocement production: A comprehensive review. *World J. Microbiol. Biotechnol.* **2025**, *41*, 67. [CrossRef] [PubMed]
34. Alotaibi, E.; Arab, M.G.; Abdallah, M.; Nassif, N.; Omar, M. Life cycle assessment of biocemented sands using enzyme induced carbonate precipitation (EICP) for soil stabilization applications. *Sci. Rep.* **2022**, *12*, 6032. [CrossRef] [PubMed]
35. Hu, Y.; Li, M.; Hu, Y.; Chen, X.; Lei, H.; Sousa, R.L. Ground settlement induced by piggyback shield tunnelling in spatially variable soils: 3D random finite-element modelling. *J. Rock. Mech. Geotech. Eng.* **2025**, *in press*. [CrossRef]

Disclaimer/Publisher's Note: The statements, opinions and data contained in all publications are solely those of the individual author(s) and contributor(s) and not of MDPI and/or the editor(s). MDPI and/or the editor(s) disclaim responsibility for any injury to people or property resulting from any ideas, methods, instructions or products referred to in the content.